Visible-enhanced photocatalytic performance of CuWO4/WO3 hetero-structures

Salimi, Reza; Sabbagh Alvani, A. A.; Naseri, N.; Du, Shangfeng; Poelman , Dirk

DOI:
10.1039/C8NJ01656A

Document Version
Peer reviewed version

Citation for published version (Harvard):
Salimi, R, Sabbagh Alvani, AA, Naseri, N, Du, S & Poelman , D 2018, 'Visible-enhanced photocatalytic performance of CuWO4/WO3 hetero-structures: incorporation of plasmonic Ag nanostructures', *New Journal of Chemistry*, vol. 42, pp. 11109-11116. https://doi.org/10.1039/C8NJ01656A

Visible-enhanced Photocatalytic Performance of $CuWO_4/WO_3$ Heterostructure: Incorporation of Plasmonic Ag Nanostructures

R. Salimi[1], A.A. Sabbagh Alvani[*,1], N. Naseri[2], S.F. Du[3], D. Poelman[4]

[1] Color & Polymer Research Center, Amirkabir University of Technology (Tehran Polytechnic), P.O. Box 15875-4413, Tehran, Iran

[2] Department of Physics, Sharif University of Technology, Tehran, Iran

[4] School of Chemical Engineering, University of Birmingham, Birmingham, UK

[4] LumiLab, Department of Solid State Sciences, Ghent University, Belgium

Tel: (+98-21) 66418600

Fax: (+98-21) 66418601

** Corresponding author E-mail:* sabbagh_alvani@aut.ac.ir

Abstract

A new plasmonic Ag hybridized $CuWO_4/WO_3$ heterostructured nanocomposite was successfully synthesized via ligand-assisted sol gel method. The as-prepared plasmonic nanohybrid was thoroughly characterized by X-ray diffraction (XRD), scanning electron microscopy (SEM), UV-visible optical absorption, photoluminescence (PL) spectrometer, Raman spectroscopy and electrochemical impedance spectroscopy (EIS). Moreover, the photocatalytic activity was evaluated by photo-degradation of methylene blue (MB) under visible light irradiation. The results indicated that the as-prepared plasmonic Ag-$CuWO_4/WO_3$ nanohybrid (compared to pure WO_3) exhibits significant enhancement in photocatalytic behavior (70% degradation) in the visible spectrum which can be ascribed to combined effects, including the more effective absorption of visible light, lower bulk resistance, effective separation/transfer of photo-generated charge carriers and reduced the electron/hole recombination which results from contribution of hetero-junction and plasmonic Ag incorporation. In addition, a possible mechanism for the photo-degradation process of hetero-structured Ag nanohybrid is proposed. Finally, the metal/semiconductor nanohybrid displayed sufficient recyclability with respect to photocatalytic activity, making it a promising candidate for pollutant degradation and energy conversion applications.

Keywords: *Visible Light Photocatalysis, Nanohybrid, Surface Plasmon Resonance (SPR), Heterostructure, Ag Nanostructures, Electronic Band Structure*

1. Introduction

Semiconductor-based photocatalysis, as an efficient and environment-friendly technique, has received considerable attention due to its several technological applications such as pollutant degradation and solar energy conversion/storage to overcome environmental pollution and global energy crisis [1-5]. In recent years, tungstate oxide materials, particularly WO_3 and $CuWO_4$, have been considered with extensive scientific research due to their suitable photo-physical properties, sufficient chemical and thermal stability, relatively low cost and less toxicity. Although WO_3 presents good electron transport properties, a relatively high resistance against photo-corrosion and moderate hole diffusion length compared to other oxides such as Fe_2O_3 and TiO_2, its photocatalytic efficiency is greatly hindered because of high recombination ratio of photo-induced electron-hole pairs, very poor response to visible light and relatively low chemical stability under neutral or basic conditions. $CuWO_4$ as compared to WO_3 is more stable against photo-corrosion in aqueous solution, and this semiconductor can more effectively harvest visible light and shows high chemical stability due to hybridized Cu-3d and O-2p orbitals. However, relatively slow charge carrier separation/mobility and rapid charge recombination of $CuWO_4$ contribute a poor overall photocatalytic efficiency [6-9]. Therefore, such limitations must be overcome to utilize these materials as ideal photocatalysts for different commercial applications. A variety of strategies have been reported to modify charge separation, carrier transport and visible absorption properties of semiconductors for tangible enhancement of photocatalytic performance [10-15]. Among these techniques, creating hetero-structured systems and incorporation of plasmonic nanostructures, as potential approaches, have been considered to overcome the different drawbacks of pure photocatalysts. In this regard, heterostructured composites not only could expand the spectral range of light absorption but also promote charge separation and chemical stability, thus quenching

the drawbacks of separate semiconductors. Moreover, noble metals, such as silver (Ag) nanostructures with surface plasmon resonance (SPR) effect, could broaden the absorption of semiconductor to the visible light region and promote the charge transfer/separation efficiency of photo-generated e/h pairs [16-22]. Therefore, in this work, we attempt to explore spontaneous formation of $CuWO_4/WO_3$ hetero-structured photocatalyst via PVP-assisted sol-gel approach and the visible enhanced photocatalytic performance of $CuWO_4/WO_3$ composite by incorporation of plasmonic silver nanostructures is comprehensively investigated. Our work provides a helpful insight to design highly efficient plasmonic metal/heterostructured nanohybrids for potential applications.

2. Experimental Procedure

2.1. Materials

Chemically high purity grade (99%, Sigma-Aldrich) ammonium metatungstate hydrate (AMT), $Cu(NO_3)_2.3H_2O$, Polyvinyl pyrrolidone (PVP, M_w = 29000 and 40000), silver nitrate ($AgNO_3$), , Iron(III) chloride ($FeCl_3$) and ethylene glycol (EG) were used as raw materials.

2.2. Ag Nanostructured Synthesis

The procedure was briefly described as follows: 10 mL of EG as reducing agent and solvent was refluxed in a three-necked round-bottom flask at 155 °C (equipped with magnetic stirring bar). 5 mL of $FeCl_3$ solution (0.1 mM, in EG) was added to the refluxing solution and reacted for 10 min to be formed heterogeneous nucleation seeds. Silver nitrate solution measuring 5 mL (0.1 M, in EG) and PVP solution were simultaneously injected dropwise into the hot solution. The reaction mixture was heated for 70 min at 155°C. And then, obtained gray suspension was cooled to room temperature, diluted with acetone and ethanol, and centrifuged several times at 4000 rpm for 10 min.

2.3. $CuWO_4/WO_3$ Synthesis

In this PVP-assisted sol-gel procedure, the final product was produced by dissolving 0.242 g $Cu(NO_3)_2.3H_2O$ in 15 mL of ethylene glycol. Next, 0.296 gr of tungsten was added as AMT, along with 1 mL of water and PVP. This mixture was then stirred, allowing the solid AMT and PVP to dissolve. The solution was then heated at 95°C in an oil bath for approximately 6 hours until it became green suspension. After centrifugation and washing, obtained powder were calcined at 525°C for 90 min in air atmosphere. For preparation of Ag nanohybrid, 5 (%w) of derived Ag

solution added to sol-gel derived product in EG under stirring for 5 hours followed by sonication for 30 min and finally heated at 160 °C for 3 hours.

2.4. Materials Characterization

In order to characterize the products, X-ray diffraction (XRD, Inel, EQuniox 3000), UV-Vis spectrophotometer (Perkin Elmer Lambda 40), scanning electron microscopy (SEM, Seron Technologies AIS2100), Raman Spectroscopy (Bruker, Senterra), Photoluminescence (PL) spectrophotometer (Perkin-Elmer LS-55) and N_2 adsorption/desorption apparatus (ASAP 2010) were all used.

2.5. Photocatalytic and Electrochemical Characterizations

The photocatalytic ability of products was evaluated by degradation of MB under a 200 W Xenon lamp irradiation with a UV cut-off filter. 40 mg the as-prepared powder was dispersed in MB solution (100 mL, 10 mg L^{-1}) in a beaker. After 30 min stirring in dark to establish adsorption-desorption equilibrium, a series of aqueous samples were collected and centrifuged at 8000 rpm for 10 min to remove essentially all of the catalyst. Then, the photo-degradation efficiency was quantified by monitoring the MB concentration of supernatant at its maximum of absorption (λ = 665 nm) by a UV-Vis spectrophotometer. The electrochemical impedance spectroscopy (EIS) analysis of the as-prepared samples were conducted by a typical three-electrode Autolab electrochemical system (PGSTAT302N) at an amplitude of 10 mV and over frequency range of 0.1 Hz to 100 kHz.

3. Results and discussion

3.1. Materials Characterization

SEM image and XRD pattern of the as-synthesized silver nanostructures are depicted in Fig. 1 which show the formation of face centered cubic (FCC) phase (a = 4.086 Å, JCPDS file number 04-0783) of silver nanostructures (nanowires and nanoparticles). PVP molecules, as capping ligand and shape-directing agent, plays a key role in the anisotropic confinements during growth process of Ag nanowires. Furthermore, the plasmonic properties of the as-prepared Ag nanostructures are confirmed by UV-Visible spectra (Fig. 1c) displaying a dual peak line shape absorption ascribed to the transverse dipole resonance (longer wavelength, λ=420 nm) and the transverse quadrupole resonance (shorter wavelength, λ=380 nm).

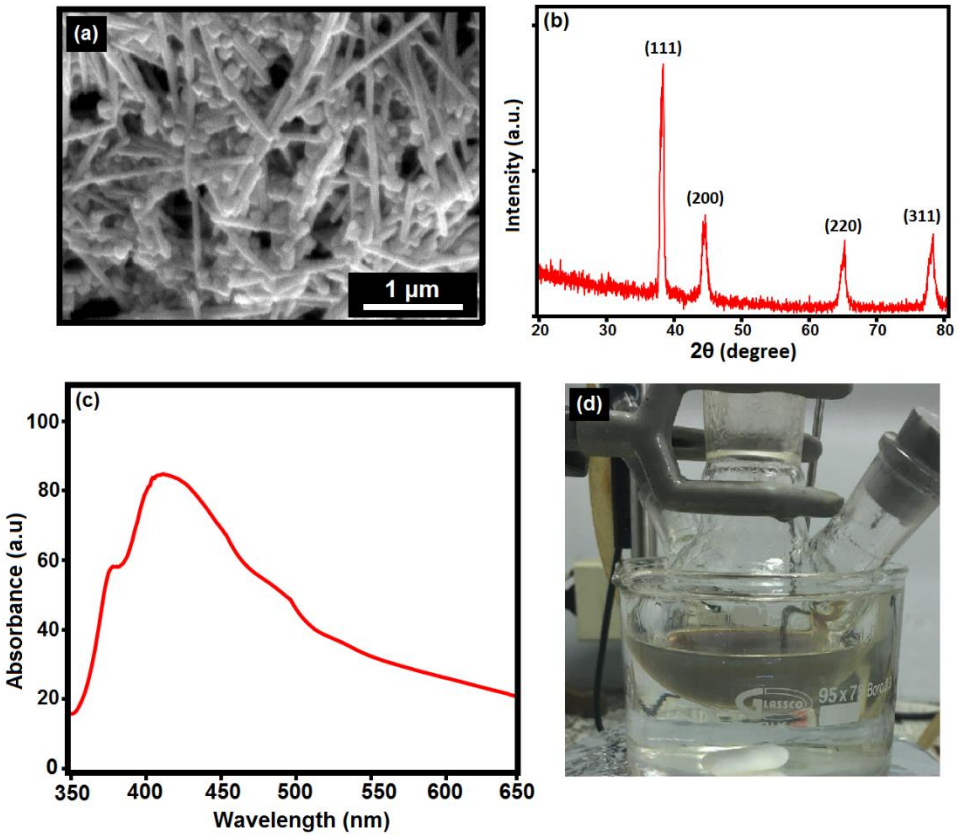

Figure 1. SEM image (a) XRD pattern (b) UV-Vis spectrum (c) of the as-synthesized Ag nanostructures (d)

Fig. 2a shows the XRD patterns of the as-obtained pure WO_3, $CuWO_4/WO_3$ hetero-structure and Ag nanohybrid. The X-ray diffraction peaks have been indexed to the both monoclinic structure of WO_3 (JCPDS data card No. 43-1035) and the triclinic structure of $CuWO_4$ (JCPDS data card No. 72-0616). The Ag nanohybrid pattern showed some new peaks that were not present in that of pure hetero-structure product. The peaks at 38.1, 44.8 and 64.2 were assigned to the (111), (200), (220) and (311) planes of face-centered cubic (FCC) Ag (JCPDS card no. 04-0783), respectively, which confirmed silver phase was introduced into the hybrid structures successfully. With the full width at half-maximum (FWHM) of the main diffraction peaks, the average crystallite size was determined to be 24-30 nm using Scherrer formula [23,24] which demonstrates that sample obtained via PSG route have low mean crystallite size which can correspond to effective role of PVP on controlling the growth process.

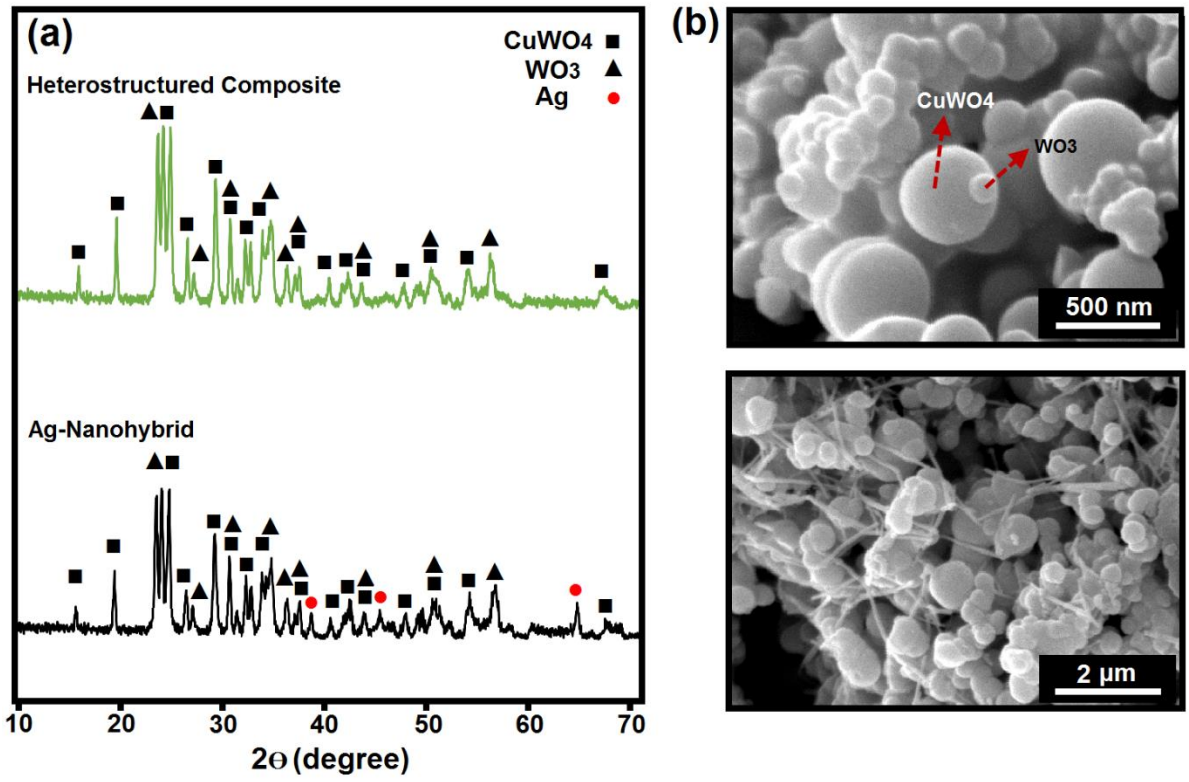

Figure 2. XRD patterns (a) and SEM images (b) of the as prepared nanocomposite and nanohybrid

Fig. 2 depicts the representative SEM micrographs of nanocomposite and nanohybrid. As shown in Fig. 2b, the composite particles obtained via PSG approach seem to have uniform spherical shaped morphology with particle sizes ranging from 100 nm (WO_3 phase) to 500 nm ($CuWO_4$ phase). The addition of PVP as chelating and surface-passivating ligand with C-O groups, not only can coordinates metal atoms, causing homogeneity in metal atom distribution in sol and gel, but also stabilizes particle growth by surrounding the particles with its long polymeric chains, leading to homogeneity of primary microparticles without significant agglomerations during sintering process. This in turn leads to high surface area which is consistent with Brunauer-Emmett-Teller (BET) analysis results with a type IV adsorption classification and 58.2 m^2/g BET surface area (Fig. 3a). The large BET surface area of the nanocomposite is beneficial for its photocatalytic activity. Moreover, SEM images show that the structure of Ag nanowires in the photocatalyst were maintained and Ag nanostructures were uniformly distributed in the nanohybrid.

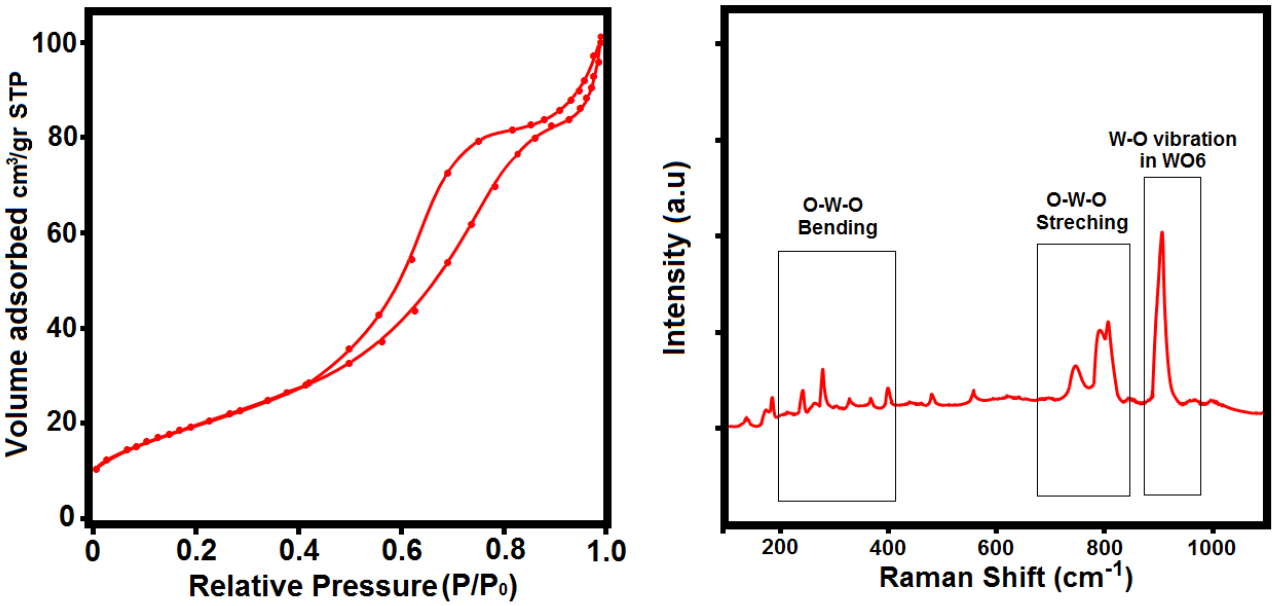

Figure 3. Nitrogen adsorption-desorption isotherm (a) and Raman spectrum (b) of the as-prepared nanohybrid

The main Raman bands of the as-prepared nanohybrid (presented in Fig. 3b) are attributed to the characteristic $CuWO_4/WO_3$ phases, which demonstrates some prominent peaks in the measured range 100-1100 cm^{-1}, attributed to the stretching vibration ν_1 (A_g) of the O-W-O bond (the strongest band), ν_2 (A_g) and ν_3 (E_g) vibration of W-O and bending modes of the O-W-O. Furthermore, the Raman spectra of $CuWO_4$ can be interpreted in terms of internal and external modes of the WO_6 octahedra. Internal modes correspond to vibrations of O atoms against W inside the WO_6 octahedra and external modes imply the movement of WO_6 octahedra as rigid units against Cu [25, 26]. Although the Raman spectra did not exhibit the significant signals related to Ag nanocrystals, the presence of Ag nanostructures cause a relative decrease in the intensity and a slight red shift of the bands relevant to composite due to an interaction between Ag and semiconductors so as to influence the resonant Raman effect for composite.

3.2. Photo-physical and Electrochemical characterization

The UV-visible spectra of the as-synthesized $CuWO_4/WO_3$ composite and Ag-nanohybrid are depicted in Fig. 4a. There are two overlapped bands below 550 nm, which was assigned to a W (5d) O(2p) ligand to metal charge transfer (LMCT) band centered about 390 nm and a W (5d)) Cu (3d) metal to metal charge transfer (MMCT) band centered about 440 nm. Compared to the WO_3 band gap (about 2.61 eV), the band-gap of the as-prepared composite and nanohybrid were estimated to be about 2.32 and 2.25 eV, respectively, indicating the hetero-structure construction effectively narrows the bang gap and improves light harvesting in the visible region. The metal Cu^{2+} d-orbitals are sufficiently low in energy as to effectively hybridize with the O (2p) valence band, which results in the lower band gap relative to that of pure WO_3. Moreover, the more effective absorption band and extending the visible light response of Ag-PSG nanohybrid at

approximately 420 nm, was mainly ascribed to the surface plasmon resonance (SPR) originating from the plasmonic nanostructures in the product.

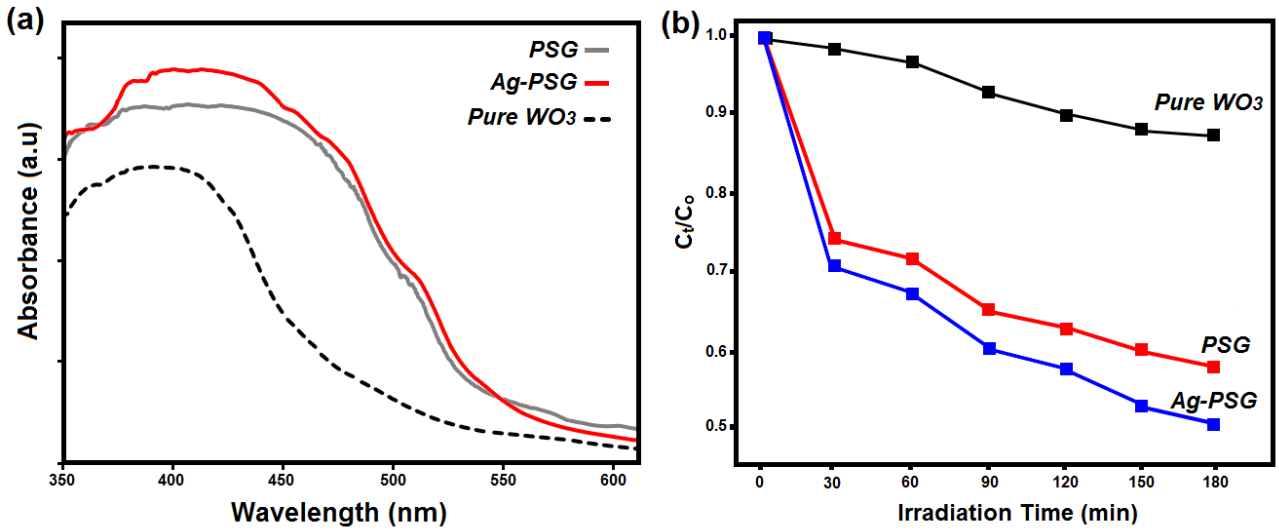

Figure 4. UV-Vis spectra (a) and photocatalytic activity (b) of the obtained products

The photocatalytic activity of the as-synthesized heterostructured composite, Ag nanohybrid and pure WO_3 was studied for the degradation of MB dye under visible irradiation, as presented in Fig. 4b. As expected, nanohybrid and heterostructured composite exhibit remarkable improvement in photocatalytic activity in comparison with the pure WO_3 [27]. It can be attributed to the formation of a nanoheterostructure between the $CuWO_4$ and WO_3 nanoparticles and the creation of an internal electric field at the interface region, improving charge transfer/separation between two phases, suppressing electron-hole recombination. Moreover, the results clearly indicate that the photo-degradation of the Ag-nanohybrid reaches 51%, more efficient than that of heterostructured composite after 3 h visible light irradiation, which can be ascribed to SPR effect of Ag nanostructures on the enhancement of visible absorption and charge carrier transfer/separation efficiency.

The PL technique is useful for disclosing the migration, transfer, and recombination processes of the photo-generated electron-hole pairs in the as synthesized products. According to Fig. 5a, it is apparent that the pure WO_3 display highly intense and broad PL band signals in the 400-600 nm region, which could be corresponded to the radiative recombination of self-trapped excitons. However, the radiative emission peaks of heterostructured composite and Ag-nanohybrid are obviously suppressed. The quenching behavior revealed that the hetero-structure and Ag nanostructures trap or transfer photogenerated charge carriers to suppress electron-hole recombination. The effective charge carrier separation could extend the reactive electron-hole pairs lifetimes and enhance the photocatalytic activity of nanohybrid. Additionally, the formation of Schottky junction in Ag nanohybrid system prohibited photo-induced carrier recombination due to the SPR effect. It should be noted that both of Ag nanowires and nanocrystals could react as electron traps, facilitating the photo-generated electrons transfer and charge carrier separation.

Nyquist plots of the EIS spectra for pure WO_3, heterostructured composite and Ag nanohybrid are presented in Fig. 5b which display typical semicircles. The diameter of the semicircles are related to the charge-transfer resistance at the electrode/electrolyte interface. According to Nyquist plots in the medium frequency range (10-10^5 Hz), the Ag nanohybrid shows a lower charge transfer resistance, which can accelerate the charge separation and inhibit the recombination between charge carriers.

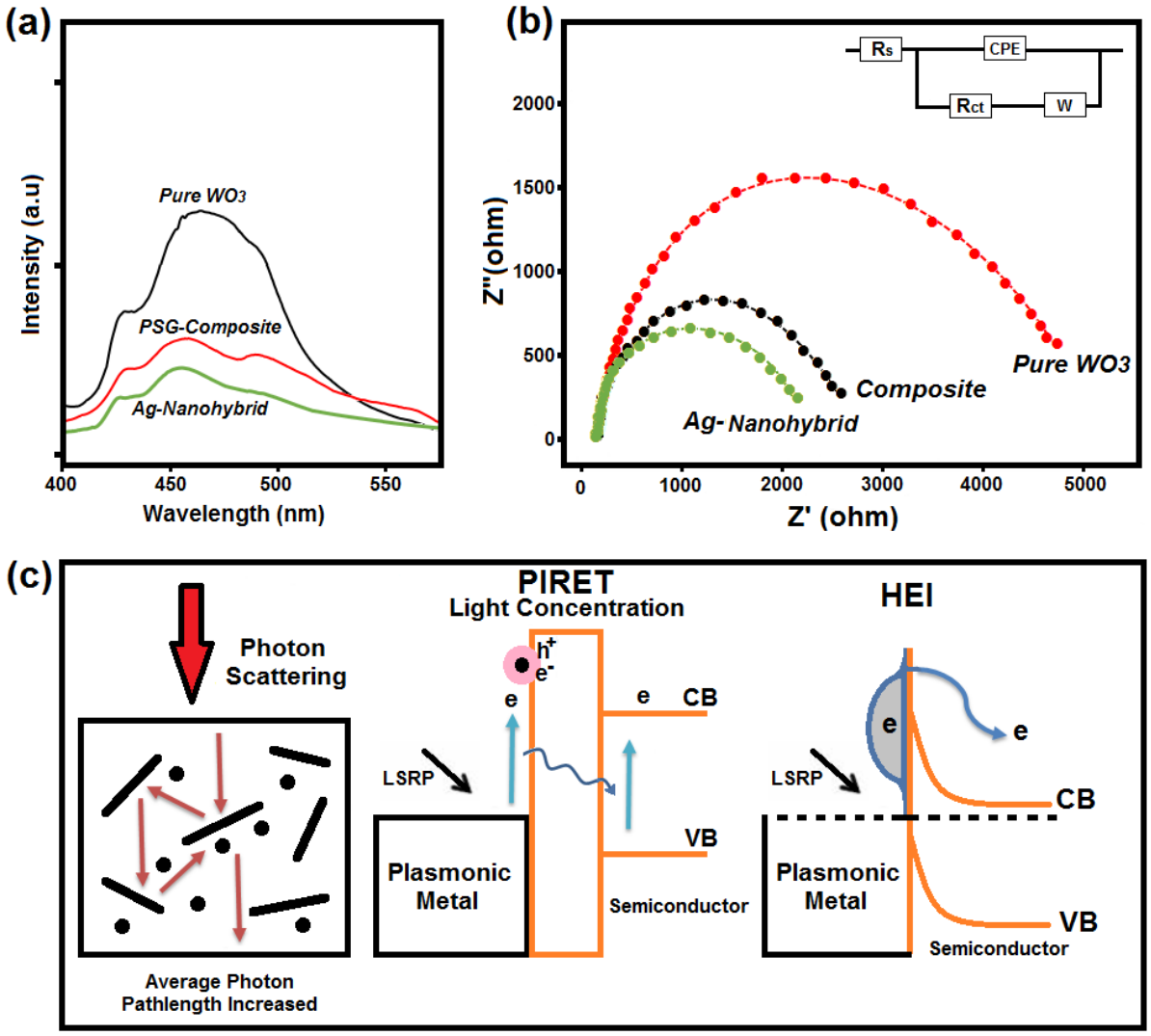

Figure 5. (a) PL spectra and (b) Nyquist plots of the as-synthesized products. (c) Different SPR effects in plasmonic-semiconductor nanohybrids

Ag nanostructures able to absorb visible light due to the existence of a localized surface plasmon resonance (LSPR). LSPR in Ag nanostructures can contribute a neighboring semiconductor in light absorption and charge separation for photocatalytic applications through four types of enhancement mechanisms: light scattering, light concentration, hot electron injection (HEI), and plasmon-induced resonance energy transfer (PIRET). Light scattering by radiative decay can

increase the effective optical path length in the semiconductor. This leads to corresponding enhanced absorption and creation of charge carriers. When the surface plasmon decays by exciting an electron-hole pair within the nanostructures (non-radiative decay), hot electrons can be transferred to the conduction band of the semiconductor and carry out the corresponding reactions. In the third (light concentration) and fourth (PIRET) mechanisms, the highly localized electric field enhancement (i.e. near-field) around the plasmonic nanostructures induces interband excitations in a neighboring semiconductor, increasing the electron-hole generation rate in the semiconductor. Unlike the HEI mechanism, the light scattering, light concentration and PIRET mechanisms do not transfer the plasmon energy by charge transfer, but radiatively or by a dipole-dipole interaction, inducing interband excitations in a neighboring semiconductor. Accordingly, during visible light irradiation, on the one hand, the Ag nanocrystals are photoexcited owing to the plasmon resonance. Subsequently, the photoexcited electrons are migrated from the surface of the Ag nanocrystals to the conduction band of semiconductors. Meanwhile, owing to the high crystallinity and conductivity of the Ag nanostructures, the resistance to electron migration is relatively low so as to reduce the recombination of e/h pairs [28-29].

The capability of a photocatalyst to function in photocatalytic applications can be photo-physically evaluated via the band edge positions. Regarding the redox potentials of MB, the positions of electronic band edges of a semiconductor identify its ability to undergo photo-induced electron transfer to the species adsorbed on the surface of photocatalyst. We predicted band edge position of photocatalysts according to a semi-empirical technique proposed by Butler and Ginley [30, 31]. According to the method, the band edge positions of a semiconductor at the point of zero charge can be expressed empirically by:

$$E_V = \chi - Ee + 0.5\, E_g \qquad (1)$$

$$E_C = E_V - E_g \quad (2)$$

$$\chi \approx \left(\prod_{k=1}^{P} \chi_k\right)^{\frac{1}{P}} \quad (3)$$

Where $Ee \approx 4.50$ eV is the scale factor relating the reference electrode redox level to the vacuum level and E_g is the band gap. The absolute electronegativity of a semiconductor, χ, defined as the geometric mean of the electronegativity of the constituent atoms. Based on the above characterization results, the enhanced photocatalytic performance of the Ag nanohybrid can be explained by a possible proposed energy band structure and photochemical reactions illustrated in Fig. 6a.

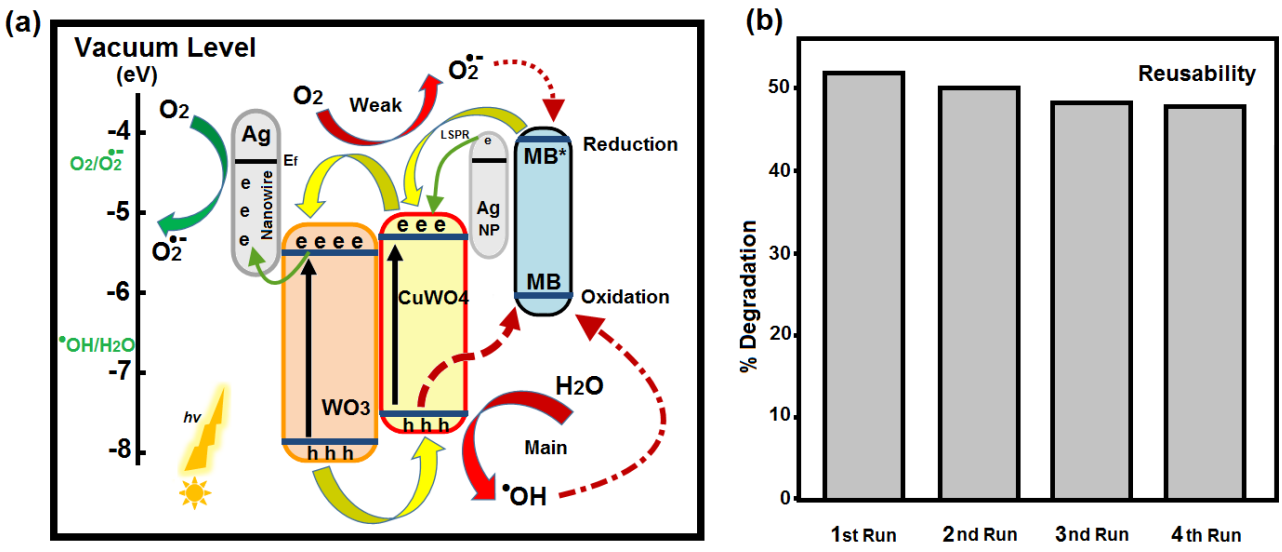

Figure 6. Photocatalysis and charge separation mechanism (a) and Reusability of the as-prepared Ag-nanohybrid (b)

Under visible light excitation, the hetero-structured composite surface generates e-h pairs, followed by rapid transfer of photo-generated electrons to Ag nanostructures and the carrier transfer between WO3 and CuWO4. Next, the negatively charged Ag nanostructures activate composite to produce $^{\bullet}O_2^-$ and holes reacts with H2O to produce •OH. Subsequently, the excited

SPR electrons in Ag NWs and nanoparticles could react with dissolved oxygen to form active oxygen species ($^{\bullet}O_2^-$), while the holes (h+) on the composite surface could easily react with water to generate $^{\bullet}$OH radicals. The holes, $^{\bullet}O_2^-$ radicals and $^{\bullet}$OH radicals played a direct or indirect role on MB degradation. Besides of the main reactions, other reactions may occur. The Ag nanohybrid could absorb visible light and then excite MB to MB*, which reacted with dissolved oxygen to produce OH-. It could further transfer to OH, which could lead to the decomposition of MB. Moreover, the excited MB can also transfer electrons to composite and Ag due to its lower work function than Ag and lying above the conduction band of composite. At the same time, the Ag^+ (h^+) ions were also reactive radical species, they were able to directly oxidize MB and reduced to metallic silver again, so the Ag could be rapidly regenerated and the composites remained stable. Meantime, the electrons generated by the LSPR effect in Ag nanostructures can overcome the energy barrier at the interface and can be injected into the CB of semiconductors. The composite function as an electron reservoir by capturing the electrons transferred from Ag to further increase the degradation efficiency of MB. Accordingly, the holes, $^{\bullet}O_2^-$ and $^{\bullet}$OH oxidize the MB molecules adsorbed on the active sites of the hetero-structured photocatalyst and Ag nanostructures. But in the case of pure hetero-structured composites, due to the fact that the CB of CuWO4 and WO3 are more positive than O2/$^{\bullet}O_2^-$, $^{\bullet}O_2^-$ is not the main active species in the photocatalytic reaction process.

Finally, the stability and reusability of the photocatalyst are very important for its practical applications. Therefore, recycling experiments on the degradation of MB by the as-synthesized Ag nanohybrid were conducted and the results are shown in Fig. 6b. It revealed that the degradation

efficiency of Ag nanohybrid decreased slightly with the recycling runs which might be attributed to insignificant photo-corrosion of nanocomposite, and the photo-degradation efficiency still kept with a slight decrease of 5.5% after 4 recycling times, indicating that the stability of the as-fabricated photocatalysts sustains its photoactivity after recycling.

Consequently, such visible enhanced photocatalytic activity of the as-prepared nanohybrid (compared to pure WO_3) is ascribed to the formation of nanoheterostructure between $CuWO_4$ and WO_3 and the SPR effects of plasmonic Ag nanostructures which improve the charge carrier pair separation efficiency. At the same time, the large surface area and more effective visible light absorption capability also contribute to the enhanced photo-catalytic activity which makes this kind of nanohybrid promising for solar energy conversion applications.

4. Conclusions

In summary, a new plasmonic Ag-$CuWO_4/WO_3$ nanohybrid, with enhanced visible light photocatalytic activity, was successfully synthesized and the photo-physical properties of the as-prepared nanohybrids were carefully investigated. The results indicated that Ag nanostructures and formation of hetero-structure are responsible for the enhancement of photocatalytic degradation performance by extending the response of nanocomposite to visible light and improving the photo-generated electrons/holes separation as well as charge migration, allowing charge carriers to partake in the overall photocatalytic reactions. Moreover, the photocatalyst reusability proved that the Ag-nanohybrid has a good stability, addressing its potential applications in pollutants removal and energy conversion.

5. Acknowledgement

The authors would like to acknowledge Color & Polymer Research Center (CPRC) and Iran Nanotechnology Initiative Council (INIC) for supporting this project.

6. References

[1] M. G. Walter, E. L. Warren, J. R. McKone, S. W. Boettcher, Q. Mi, E. A. Santori, N. S. Lewis, Solar water splitting cells, Chem. Rev. 110 (2010) 110, 6446-6473

[2] M. Gholami, M. Qorbani, O. Moradlou, N. Naseri, A. Z. Moshfegh, Optimal Ag_2S nanoparticle incorporated TiO_2 nanotube array for visible water splitting, RSC Adv. 4 (2014) 7838-7844

[3] R. Velmurugan, B. Sreedhar, M. Swaminathan, Nanostructured AgBr loaded TiO_2: An efficient sunlight active photocatalyst for degradation of Reactive Red 120, Chem.Cent. J. 5:46 (2011) 1-9.

[4] X. Liu, Y. Kang, Synthesis and high visible-light activity of novel $Bi_2O_3/FeVO_4$ heterojunction photocatalyst, Mater. Lett. 164 (2016) 229-231

[5] H. Sameie, A.A. Sabbagh Alvani, N. Naseri, S. Du, F. Rosei, First Principles study on ZnV_2O_6 and Zn_2V2O_7: Two new photoanode candidate for photoelectronchemical water oxidation, Ceram. Int. 44 (2018) 6607-6613

[6] A. M. Cruz, D. S. Martınez, E. L. Cuellar, Synthesis and characterization of WO_3 nanoparticles prepared by the precipitation method: Evaluation of photocatalytic activity under vis-irradiation, Solid State Sci. 12 (2010) 88-94

[7] X. Xie, M. Lu, C. Wang, L. Chen, J. Xu, Y. Cheng, H. Dong, F. Lu, W. H. Wang, H. Liu, W. Wang, Effcient photo-degradation of dyes using $CuWO_4$ nanoparticles with electron sacrificial agents: a combination of experimental and theoretical exploration, RSC Adv. 6 (2016) 953-959.

[8] W. Ye, F. Chen, F. Zhao, N. Han, and Y. Li, $CuWO_4$ Nanoflake Array-Based Single-Junction and Heterojunction Photoanodes for Photoelectrochemical Water Oxidation, ACS Appl. Mater. Interfaces. 8 (2016) 9211-9217

[9] J. Liu, S. Han, J. Li, Jun Lin, Modification of tungsten trioxide with ionic liquid for enhanced photocatalytic performance, RSC Adv. 4 (2014) 37556-37562

[10] J. Xie, Z. Zhou, Y. Lian, Y. Hao, X. Liu, M. Li, Y. Wei, Simple preparation of WO_3-ZnO composites with UV-Vis photocatalytic activity and energy storage ability, Ceram. Int. 40 (2014) 12519-12524

[11] S. S. Kalanur, I. Yoo, H. Seo, Fundamental investigation of Ti doped WO_3 photoanode and their influence on photoelectrochemical water splitting activity, Electrochim. Act. 254 (2017) 348-357

[12] Sh. Bai, K. Zhang, J. Sun, R. Luo, D. Li, A. Chen, Surface decoration of WO_3 architectures with Fe_2O_3 nanoparticles for visible-light-driven photocatalysis, CrystEngComm. 16 (2014) 3289-3295

[13] D. Bohra and W. A. Smith, Improved charge separation via Fe-doping of copper tungstate photoanodes, Phys. Chem. Chem. Phys. 17 (2015) 9857-9866

[14] S. K. Pilli, J. A. Turner, T. G. Deutsch, A. M. Herring, T. E. Furtak, L. D. Brown, $BiVO_4/CuWO_4$ hetero-junction photoanodes for efficient solar driven water oxidation, Phys. Chem. Chem. Phys. 15 (2013) 3273-3278

[15] H. Chen, W. Leng, Y. Xu, Enhanced Visible-Light Photoactivity of $CuWO_4$ through a Surface Deposited CuO, J. Phys. Chem. C. 118 (2014) 9982-9989

[16] L. Gan, L. Xu, S. Shang, X. Zhou, L. Meng, Visible light induced methylene blue dye degradation photo-catalyzed by WO_3 /Graphene nanocomposites and the mechanism, Ceram. Int. 42 (2016) 15235-15241.

[17] L.C. Sim, K.H. Leong, S. Ibrahim, P. Saravanan, Graphene oxide and Ag engulfed TiO_2 nanotube arrays for enhanced electron mobility and visible light-driven photocatalytic performance, J. Mater. Chem. A. 2 (2014) 5315-5322

[18] H. Liu, T. Liu, X. Dong, R. Hua, Z. Zhu, Preparation and enhanced photocatalytic activity of Ag-nanowires@SnO_2 core-hell heterogeneous structures, Ceram. Int. 40 (2014) 16671-16675

[19] D. Wang, P.S. Bassi, H. Qi, X. Zhao, L. H. Wong, R. Xu, T. Sritharan, Z. Chen, Improved Charge Separation in $WO_3/CuWO_4$ Composite Photoanodes for Photoelectrochemical Water Oxidation, Materials. 9 (2016) 348-360

[20] J. E. Yourey, J. B. Kurtz, B. M. Bartlett, Water Oxidation on a $CuWO_4$-WO_3 Composite Electrode in the Presence of $[Fe(CN)6]^{-3}$: Toward Solar Z-Scheme Water Splitting at Zero Bias, J. Phys. Chem. C. 116 (2012) 3200-3205

[21] C. Su, L. Liu, M. Zhang, Y. Zhang, C. Shao, Fabrication of Ag/TiO_2 nanoheterostructures with visible light photocatalytic function via a solvothermal approach, CrystEngComm. 14 (2012), 3989-3999

[22] H. Liu, C. Hu, H. Zhai, J. Yang, X. Liu, H. Jia, Fabrication of In_2O_3/ZnO@Ag nanowire ternary composites with enhanced visible light photocatalytic activity, RSC Adv. 7 (2017) 37220-37229.

[23] A. L Patterson, The Scherrer Formula for X-Ray Particle Size Determination, Phys. Rev. 56 (1939) 978-982.

[24] R. Salimi, H. Sameie, AA. Sabbagh Alvani, AA. Sarabi, F. Moztarzadeh, H. Mohammadloo, F. Nargesian, M. Tahriri, Sol-gel synthesis, structural and optical characteristics of $Sr_{1-x}Zn_2Si_2yO_{7+\delta}$: xEu^{2+} as a potential nanocrystalline phosphor for near-ultraviolet white light-emitting diodes, J. Mater. Sci. 47 (2012) 2658-2664

[25] R.K. Selvan, A. Gedanken, The sonochemical synthesis and characterization of $Cu_{1-x}Ni_xWO_4$ nanoparticles/nanorods and their application in electrocatalytic hydrogen evolution, Nanotech. 20 (2009) 105602-105609

[26] F. Liu, X. Chen, Q. Xia, L. Tian, X. Chen, Ultrathin tungsten oxide nanowires: oleylamine assisted nonhydrolytic growth, oxygen vacancy and high photocatalytic properties, RSC Adv. 5 (2015) 77423-77428

[27] M. Dinari, M. M. Momeni, M. Ahangarpour, Efficient degradation of methylene blue dye over tungsten trioxide/multi-walled carbon nanotube system as a novel photocatalyst, Appl. Phys. A. 876 (2016) 1-9

[28] S. Linic, P. Christopher, D. B. Ingram, Plasmonic-metal nanostructures for efficient conversion of solar to chemical energy, Nat. Mater. 10 (2011) 911-921.

[29] J. Li, S.K. Cushing, F. Meng, T.R. Senty, A.D. Bristow, N. Wu, Plasmon-induced resonance energy transfer for solar energy conversion, Nat. Photonics. 9 (2015) 601-608

[30] M.A. Butler, D.S. Ginley, Prediction of flatband potentials at semiconductor-electrolyte interface from atomic electronegativitics. J. Electrochem. Soc. 125 (1978) 228-232.

[31] J. Liu, S. Chen, Q. Liu, Y. Zhu, Y. Lu, Density functional theory study on electronic and photocatalytic properties of orthorhombic $AgInS_2$, Comput. Mater. Sci. 91 (2014) 159-164.